Organic Electronics 13 (2012) 235–243

Contents lists available at SciVerse ScienceDirect

Organic Electronics

journal homepage: www.elsevier.com/locate/orgel

Fabrication of organic semiconductor crystalline thin films and crystals from solution by confined crystallization

Hylke B. Akkerman [a], Alice C. Chang [a], Eric Verploegen [a,b], Christopher J. Bettinger [a,1], Michael F. Toney [b], Zhenan Bao [a,*]

[a] Stanford University, Department of Chemical Engineering, Stauffer III, 381 North-South Mall, Stanford, CA 94305-5025, USA
[b] Stanford Synchrotron Radiation Lightsource, 2575 Sand Hill Rd., Menlo Park, CA 94025, USA

ARTICLE INFO

Article history:
Received 15 September 2011
Received in revised form 13 November 2011
Accepted 15 November 2011
Available online 29 November 2011

Keywords:
Organic electronics
Field-effect transistors
Crystals
Crystalline thin films
Single-crystal devices
TIPS-pentacene

ABSTRACT

Highly crystalline thin films of organic semiconductors processed from solution for electronic devices are difficult to achieve due to a slow and preferential three-dimensional growth of the crystals. Here we describe the development of a processing technique to induce a preferential two-dimensional crystalline growth of organic semiconductors by means of minimizing one dimension and confining the solution in two dimensions into a thin layer. The versatility of the process is demonstrated by processing small molecules (TIPS-pentacene and C_{60}) and a polymer (P3HT), all from solvents with a relatively low boiling point, to obtain crystalline thin films. The thin films show an improved in-plane packing of the molecules compared to films processed under similar conditions by spin coating, which is beneficial for the use in organic field-effect transistors.

1. Introduction

Organic field-effect transistors are of potential importance for many future electronic applications, such as displays [1,2], RFID tags [3] and sensors [4–6]. The devices with the highest field-effect mobility, a key figure of merit, are those comprising organic single crystals [7–10]. Devices based on single crystals are free of large structural defects (e.g., grain boundaries) that limit electronic transport; mobilities as high as 20 $cm^2/V\,s$ have been reported [11]. However, many techniques for single crystal devices face several limitations in processing. For example, traditional single crystal devices grown from vapor are notoriously hard to fabricate. The crystals are slowly grown from vapor in a thermal gradient furnace, visually selected and individually placed by hand on top of electrodes. This introduces a low yield and low reproducibility and, hence, makes fabrication of single crystal devices by this method unsuitable for up-scaling and implementation into existing process technology. To tackle this problem, we have previously reported processes using patterned surface modification to grow single crystals locally on top of electrode arrays [12,13]. Instead of using single crystal devices grown from vapor, crystalline films obtained from solution processing are good candidates for high performance field-effect transistors (FETs) [14–17]. The recent emergence of novel, soluble small molecules demonstrate that field-effect mobilities up to 10 $cm^2/V\,s$ can be achieved in single crystal devices from solution processing [18]. Utilizing single crystals from solution for large-area applications is challenging, but a major step forward was demonstrated by inkjet printing of single crystals by means of anti-solvent crystallization of 2,7-dioctyl[1]benzothieno[3,2-*b*][1]benzothiophene (C8-BTBT), where an average mobility of 16.4 $cm^2/V\,s$ was obtained with a peak mobility of 31.3 $cm^2/V\,s$ [19]. The fabrication of high quality crystalline films or single crystals from solution often requires a slow drying process at room temperature, due to the use

* Corresponding author. Tel.: +1 650 926 2996; fax: +1 6507239780.
E-mail address: zbao@stanford.edu (Z. Bao).
[1] Present address: Carnegie Mellon University, Department of Materials Science and Engineering, 5000 Forbes Avenue, Wean Hall 4315, Pittsburgh, PA 15213-3890, USA.

1566-1199/$ - see front matter © 2011 Elsevier B.V. All rights reserved.
doi:10.1016/j.orgel.2011.11.005

of high boiling point solvents, after which an annealing step is required for the removal of these solvents [18,20]. A technique to fabricate oriented crystalline films from solutions with a low boiling point is solution shearing [21,22]. However, due to the formation of cracks in the film, the crystal domains are limited in size in this shearing process. A technique for the fabrication of crystalline conjugated organic nanostructures is provided by lithographically controlled wetting, where by localized deposition of a material from solution nanostructured lines are formed that duplicate the stamp pattern on top [23,24]. The crystalline organic lines have a width smaller than 200 nm and showed an improved electrical transport compared to spin coated samples of the same material. Upscaling of the method to larger areas was not presented and large single crystals cannot be obtained by this method.

Therefore, a quick and simple method for the fabrication of crystalline films or crystals to test the field-effect mobility of a material needs yet to be developed. This process should require only small amounts of material per sample and should result in uniform films. The latter implies eliminating the coffee ring effect, as is often observed in drop casting due to a gradient in evaporation speed and pinning of the material at the evaporation front.

2. Results and discussion

Here, we report a technique to fabricate organic crystalline films from solvents with a low boiling point and without annealing of the films. For the deposition of the organic semiconductor, we confine the solution in the vertical direction between the substrate and a fluorinated stamp. The fabrication process for thin films in a confined space is schematically depicted in Fig. 1. First, a line pattern was fabricated in a photoresist structure, which served as a mold for the preparation of fluorinated stamps. The lines varied in width between 1 and 4 mm and have a length between 8 and 15 mm. The stamps were fabricated according to a previously published procedure for microfluidic masters made from perfluoropolyether (PFPE) [25] (Fig. 1a). PFPE stamps were used because of its resistance to organic solvents [26], while the more commonly used polydimethylsiloxane (PDMS) swells and changes shape when exposed to most organic solvents [27]. After curing, the stamps were placed on a highly doped silicon wafer with a thermally grown oxide, functionalized with hexamethyldisilazane (HMDS). The treatment with HMDS is not a prerequisite and it should be noted that we obtained similar thin films on untreated SiO_2 and glass substrates with a lower hydrophobicity. The stamps do not immediately adhere to the surface when initially placed on the substrate. The limited adhesion of the stamp to the substrate was utilized to fabricate the confined space. To wet the substrate locally, a small force was applied by hand on the sides of the stamp (Fig. 1b), thereby limiting the region for solution deposition to be between the sides contacting the substrate. Furthermore, adhesion of the sides of the stamp ensures that the stamp remains in place while depositing the solution. Due to the limited adhesion of the PFPE stamps on the HMDS-treated SiO_2, the middle region of the stamp (hereafter called the channel) is not in close contact with the substrate and, a small space is created that is limited in the vertical direction. The relatively high rigidity of the PFPE stamps, compared to for example PDMS, is crucial for the formation of the confined space, since it prevents the adhesion in the channel region due to bending of the stamp. The exact height of the confined space is unknown and will, most likely, vary slightly between different stamps. If the features next to the channel (the reservoirs) are not present, i.e., a flat stamp without any features, the whole stamp would wet the surface after pressing only a corner of the stamp. The reservoirs (as indicated in Fig. 1c) next to the channel region create the possibility of non-wetting and, therefore, a confined space between substrate and stamp.

Next, the solution of an organic semiconductor is deposited underneath the stamp by capillary forces (Fig. 1c). Due to the confined spacing between substrate and stamp in the channel region, this region is filled with solvent first before the reservoirs are filled. In fact, albeit hard to control by hand, the deposition of solvent only in the channel region is possible and the filling of the reservoirs with solvent does not seem to influence the film formation in the channel region. After about 5 min, the solvent dries and the stamp can be peeled off to expose the crystalline thin film in the channel region for the evaporation of Au source and drain electrodes.

Several factors determined the choice of materials used in this study: the polymer, regioregular poly(3-hexylthiophene) (P3HT), and the small molecules, 6,13-bis(triisopropylsilylethynyl) (TIPS) pentacene and C_{60}. The motivation for the material is presented at the beginning of each section related to that material. Here we investigate the thin film morphology of the three compounds processed by confined crystallization, along with their electrical performance in field-effect transistors.

2.1. P3HT

P3HT is known to exhibit a strong face-to-face packing of the conjugated backbone. The morphology of the film is strongly determined by the molecular weight and processing conditions [28–31]. A recent report demonstrated the possibility for P3HT to form films with a, previously unobserved, morphology from solution processing, where oriented nanofibrils are formed when the film is dried at high vapor pressure with a substrate on top [32]. Furthermore, it was shown that the chain alignment of P3HT can be influenced by confining P3HT in plane, in nanostructures fabricated by nanoimprint lithography [33]. The strong orientation and packing dependence of P3HT on varying processing conditions render the material ideal for studying the effects of confinement in the vertical direction.

Reference films were fabricated with P3HT from chloroform to compare with those made by the confined solution deposition technique under similar conditions. The width of the channel and reservoir were chosen independently, in different ratios. Typical transfer characteristics ($V_{ds} = -60$ V) of the P3HT FETs fabricated by confined crystallization, are shown in Fig. 2a. The square root of the drain

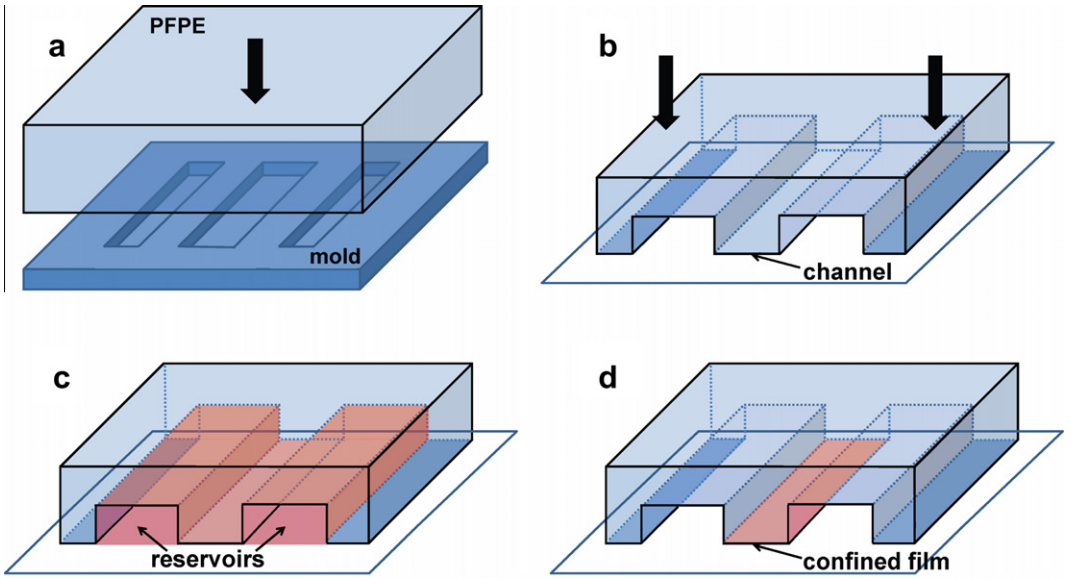

Fig. 1. A schematic overview of the fabrication of crystalline thin films in a confined space. A mold with patterned photoresist is used for the fabrication of PFPE stamps with a line pattern morphology (a). The stamp is placed on top of a substrate and the sides of the stamp are pressed to adhere to the substrate, but ensuring a non-wetting middle channel region where a confined space is remaining (b). The organic solution is deposited in the channel region and, possibly, in the reservoirs by capillary forces (c). After drying of the reservoir regions, a crystalline thin film resides in the confined channel region (d), that can be exposed for further analysis or Au source–drain contact evaporation by removing the stamp.

current ($I_{ds}^{1/2}$) was calculated and the slope of $I_{ds}^{1/2}$ versus gate voltage (V_g) was used to calculate the mobility (μ) in the saturated regime (see Supporting information for details). The average mobility from reference (spin coated) films without annealing was $\mu = (1.16 \pm 0.05) \times 10^{-3}$ cm^2/V s. The average mobility from confined deposition was more than an order of magnitude higher, i.e., $\mu = (2.7 \pm 0.8) \times 10^{-2}$ cm^2/V s. The average mobility was determined from 45 devices on nine different substrates, all with a different channel-to-reservoir width ratio to investigate its influence. The transistors showed an average on/off ratio of 2.5×10^4 and an average threshold voltage $V_t = -12 \pm 4$ V. It is noted that the mobility obtained here is not as high as some of the highest reported for P3HT [31,34,35]. It is well known that the mobility is dependent on molecular weight, annealing temperature and boiling point of the solvent [28,31,36]. However, using the same batch of polymer and solvent, the comparison between the standard spin coated devices and the confined crystalline devices is meaningful.

Fig. 2b shows the average mobility obtained per sample, plotted versus different combinations of channel and reservoir width (mm). For comparison, the average mobility from spin coating under similar conditions, denoted by sc on the *x*-axis, is plotted. There is no significant dependence

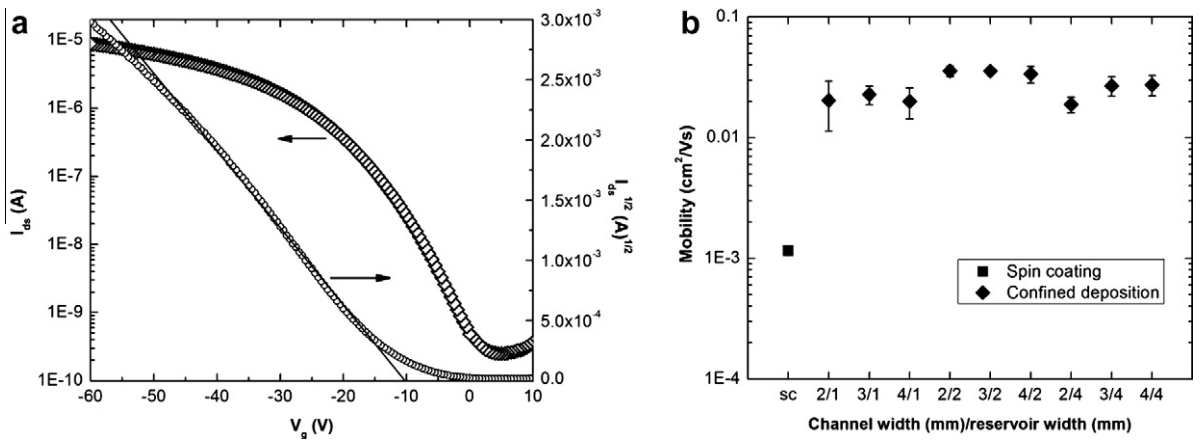

Fig. 2. Typical transfer characteristics of a FET fabricated by confined solution deposition with P3HT from chloroform, with a drain bias $V_{ds} = -60$ V (a). The highly doped Si substrate was used as a gate and 40 nm Au top source and drain electrodes were thermally evaporated through a shadow mask with $W/L = 20$ and $L = 50$ μm. (b) The mobility is plotted for different channel widths, reservoir widths and combination thereof. For comparison, the mobility obtained by spin coating (sc) under similar conditions is provided and is more than an order of magnitude lower compared to that of the confined crystalline P3HT film from chloroform.

on either channel width or reservoir width on these length scales. It should be noted that we also found good film formation when no solution was collected in the reservoirs, indicating that the presence of solution in the reservoirs does not influence the P3HT film formation in the channel region at the concentrations used here. To examine the difference between the films formed from spin coating compared to those formed in a confined space from the same solvent and batch of polymer, optical microscopy, atomic force microscopy (AFM), and grazing incidence X-ray diffraction (GIXD) were performed. Fig. 3 shows an optical micrograph at 1000× magnification (a) and the cross polarized image at the same location (b). The cross polarized image shows a locally ordered or crystalline film, with crystalline domains in the μm range. For spin coated films, a homogenous film is observed at these length scales and the film is invisible under cross polarized light (see Supporting information). The crystalline domains in the P3HT films are often arranged in a crossed pattern, where the two directions (indicated by two slightly different colors in the cross polarized image) are both under an angle of about 45° to the flow of the solution entering the confined space and, likely, drying direction.

The improved orientation by film formation in a confined space is confirmed by GIXD. Fig. S3a and b of the Supporting information shows the scattering pattern obtained from a spin coated and a confined solution deposited sample from, respectively. The most pronounced difference in these patterns is the orientation of the P3HT crystallites. The films fabricated in a confined space showed a very strong (100) texture, with the (h00) peaks aligned near the Q_z direction and the π–π stacking in the substrate plane. We can conclude that the polymer is mainly edge-on on the substrate: the backbone and π–π stacking are parallel to the substrate surface. In contrast, for the spin coated films, there is a mixed orientation with the (100) both parallel and perpendicular to the substrate. The π–π stacking peak is broad and largely out-of-plane, showing that a fraction of the polymer is face-on on the substrate surface. This is consistent with the lower mobility of the spin coated films, as now the π–π stacking direction is not in the same direction as the charge transport direction.

The morphology was subsequently studied in more detail by AFM. Fig. 4 shows the height image obtained by AFM on the spin coated (a) and confined solution deposited film (b). The spin coated film is uniform (the height scale of the AFM image in Fig. 4a is 15 nm), has small grains and has a low roughness with an RMS value of 1.3 nm. The crystalline P3HT film from confined deposition showed the similar cross-pattern structure, as observed by polarized light microscopy, as higher features (height scale of the AFM image is 50 nm). However, the macroscopic morphological structures themselves appear to consist of P3HT fibers. The clustering or bundling of P3HT fibers leads to a much larger roughness (RMS value of 6.7 nm), compared to the films formed by spin coating. In a top contact configuration in an FET, the surface roughness of the semiconductor has little effect on the charge transport, since most charge transport occurs within the first few nanometers from the dielectric/semiconductor interface [37,38]. The enhanced mobility of P3HT by confined solution deposition is, therefore, solely due to the improved orientation in the film. The increased roughness of the film when formed in a confined space is perhaps counter-intuitive. However, assuming a preferential packing and, hence, growth direction of P3HT, elongated fibers and crystalline regions can emerge during the evaporation of the solvent, leading to a non-uniform film with a higher roughness. The well-defined edge of the film, at the interface of the channel and reservoir, often shows a narrow region where f more material is deposited which originates from the reservoirs upon drying (see Fig. S4, Supporting information). The well-defined edge demonstrates that P3HT can be deposited at a specific predefined location on the substrate and that the film area is determined by the shape and dimensions of the channel region of the stamp.

2.2. TIPS-pentacene

TIPS-pentacene is known to grow into large crystals from solution under slow drying conditions [39,40]. High field-effect mobilities were reported for TIPS-pentacene films when fabricated from solvents with a high boiling point or with a controlled evaporation process and, hence,

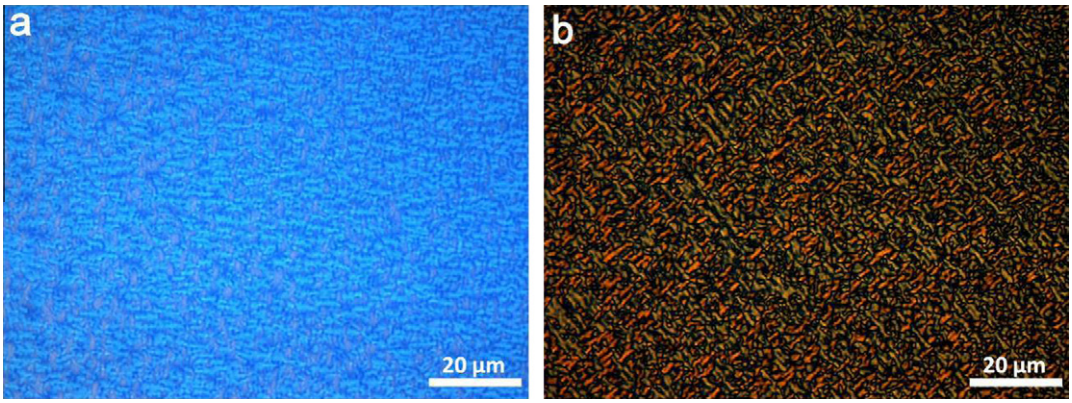

Fig. 3. An optical micrograph at 1000× magnification (a) of a P3HT film processed in confined conditions. Ordered crystalline domains are observed under cross polarized light (b), with a cross-shape morphology of several micrometers in size.

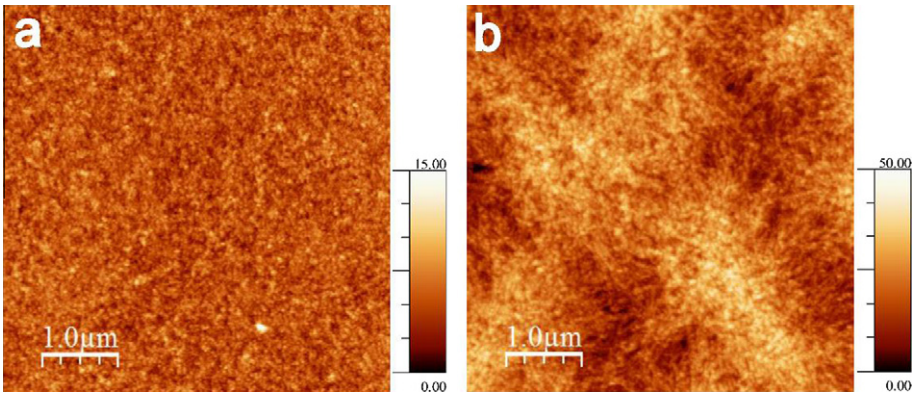

Fig. 4. AFM height images of a film by spin coating (a) and confined solution deposition (b). The crystalline P3HT film by confined solution deposition has a higher roughness due to the formation of fibers, compared to that of the spin coated film. The fibers bundle locally in two preferential directions perpendicular to each other (in the image under an angle of about 45°), to form a part of the macro scale cross-pattern features observed by polarized light microscopy.

slow crystal growth [15,40]. Therefore, we attempt to investigate the effect of using a confined geometry for film formation.

TIPS-pentacene thin films were prepared from chloroform. Transfer and output characteristics are shown in Fig. 5. An average field-effect mobility (26 devices, eight samples) $\mu = 0.29 \pm 0.14\ cm^2/V\ s$ was obtained from crystalline TIPS-pentacene by confined solution deposition. In striking contrast, the spin coated films from chloroform, without annealing gave a mobility that is about three orders of magnitude lower, $\mu = (3.4 \pm 0.5) \times 10^{-4}\ cm^2/V\ s$. Optically, the spin coated films from chloroform showed no crystalline regions or large domains, but when processed in a confined space, very large crystals emerged. Fig. 6a shows an optical micrograph of a TIPS-pentacene thin film processed from chloroform at a magnification of 25×. Elongated crystals of a few mm in length can grow in the confined space, depending on physical limitations such as the length of the stamp and distance between point of nucleation and edge of the stamp. Fig. 6b shows the same sample under cross polarized light. Different colors of the crystals correspond to different orientation or thickness. The thickness of the crystals at different locations in the film was measured by AFM and profilometry.

The orange and red colored crystals in the center of the film are of about the same thickness (~30–40 nm) but with different orientations. Upon rotating the stage under cross polarized light, the contrasts of these crystals invert. The narrow elongated crystals (Fig. 6c) are around 60–70 nm thick, depending on the location on the sample and increase in thickness towards the edge. The bigger crystals towards the edge of the film (Fig. 6d), lighter in color, are about 300 nm thick. Since the PFPE stamp on top of the substrate is transparent, we could observe the crystallization in-situ by optical microscopy. The crystal growth starts at the nucleation points at random locations in the center of the film. The initial crystal growth is dendritic and branches in all directions. Depending on the crystal size and the area available, some of the branches of the crystal continue to grow for several millimeters towards the edge of the film. The initial dendritic growth occurs in the first few seconds, when most of the

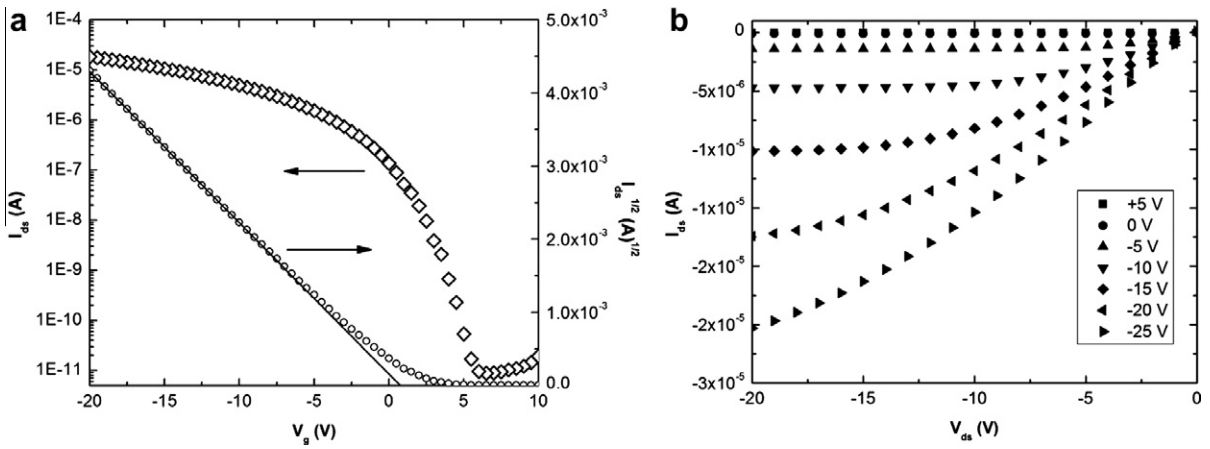

Fig. 5. Transfer characteristics ($V_{ds} = -20$ V) (a) and output characteristics (b) of a FET fabricated by confined solution deposition with TIPS-pentacene from chloroform. The saturated mobility was determined from the slope of $I_{ds}^{1/2}$ versus V_g. The average mobility was $\mu = 0.29 \pm 0.14\ cm^2/V\ s$, with an average threshold voltage $V_t = 2.1 \pm 1.2$ V and an on/off ratio of about 1×10^5.

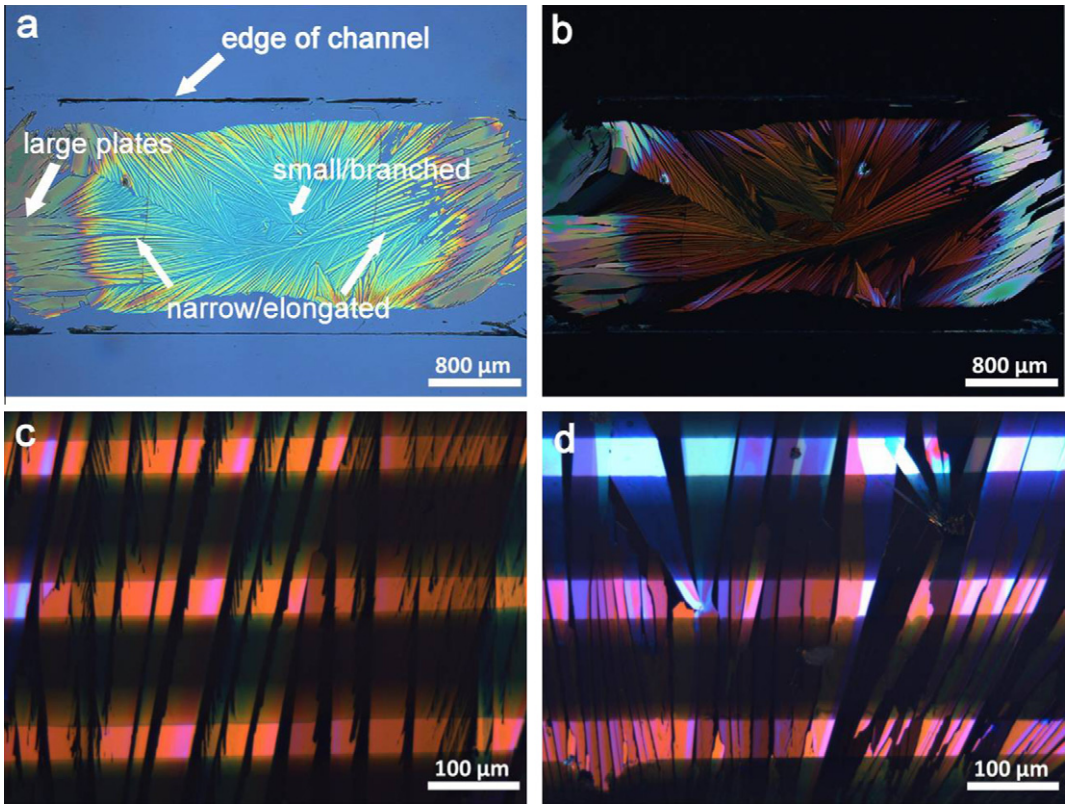

Fig. 6. An optical micrograph at 25× magnification (a) of a TIPS-pentacene film processed in confined conditions from chloroform. The different crystals observed in the film are indicated by markers in (a). Long crystals are observed under cross polarized light (b), that grow larger and thicker towards the end of the film. The single crystal nature over a length of several millimeters of some of the crystals was confirmed by rotation of the sample stage under cross polarized light, where a simultaneous extinction occurs. This can also be observed in (b), by the dark diagonal feature in the film. Au electrodes (dark horizontal lines) are evaporated on top to complete the transistor configuration (c, d) and the *W/L* is measured by optical microscopy in case of incomplete sample coverage of the film, and/or distance between electrodes.

film is formed, and the larger single crystal plates grow much slower in about 2 min. Fig. 6b shows a long dark diagonal feature which is due to extinction of light under a certain angle, indicating a single crystal orientation from the nucleation point all the way to the edge of the film. Upon rotation of the sample stage, this region will be visible and other crystals with a slightly different orientation will extinguish. The mobility obtained has quite a large spread (μ = 0.11–0.61 cm^2/V s) and depends on the crystal thickness and orientation of the crystals between the source and drain electrodes, relative to the electric field. We find the highest mobility for crystals aligned with the growth direction parallel to the electric field, with a peak mobility μ = 0.61 cm^2/V s. Although this value is lower compared to previously reported best values for TIPS-pentacene from solution (mobilities around 1–2 cm^2/V s [15,17,41,42]), it should be noted that we only varied the concentration of the solution as a process parameter. Chloroform is the preferred choice of solvent since the drying of the film occurs within a few minutes. However, initial tests using toluene as a solvent resulted in a mobility of μ = 0.94 cm^2/V s. Toluene, having a higher boiling point, takes longer to evaporate and crystals grow slower with, likely, better quality. Further optimization by using different solvents, is currently under investigation.

The TIPS-pentacene crystals grow radially outward from a nucleation point, which in combination with the elongated rectangular channel area results in crystals oriented mainly parallel to the array of source and drain electrodes, i.e., parallel to the electric field. However, close to the nucleation point this is not the case and crystals can be oriented under an angle up to 45° relative to the electric field, and still bridge the source–drain gap. Furthermore, crystals close to the nucleation point are small in size, which combined with a different orientation results in a lower value of the mobility of about 0.1 cm^2/V s. GIXD was performed to study the crystallinity relative to the spin coated films. The scattering patterns are shown in Fig. S6a and b (Supporting information). The TIPS-pentacene crystalline films fabricated in a confined space showed distinct spots in the image; this shows high crystallinity and highly oriented crystals. In contrast, the spin coasted films show arcs that result from a broad distribution of crystallite orientations. By AFM we measured the step height from two consecutive layers to be around 1.7 nm, which corresponds well with the d(001) spacing found previously for single crystal TIPS-pentacene, d(001) = 16.8–17.0 Å [43,44]. The step height from the samples in Fig. S6a and b are ~16.7 and 16.6 Å, respectively.

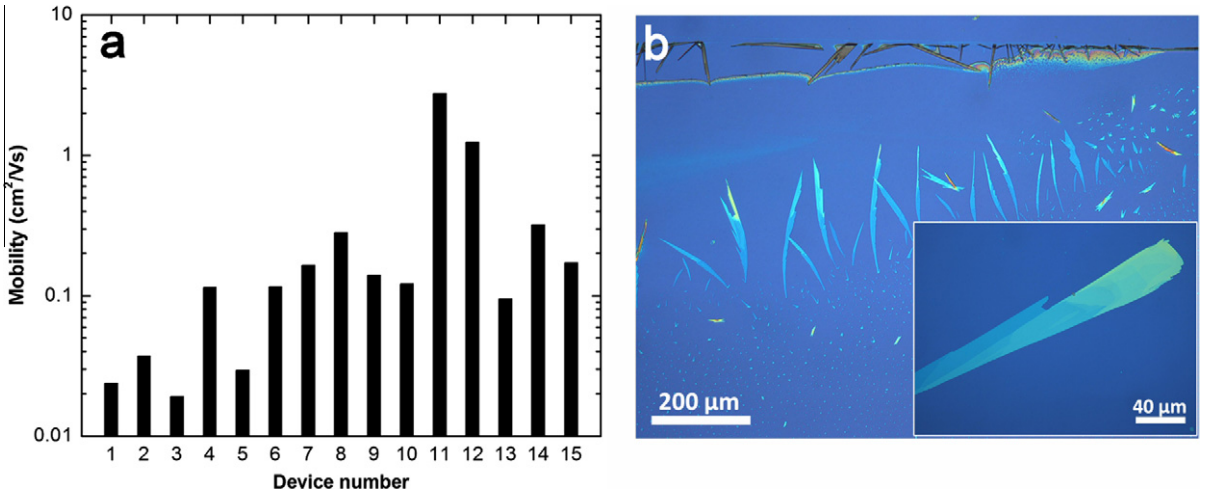

Fig. 7. The mobility of 15 devices from six different samples is plotted for C_{60} (a). Two orders of magnitude in mobility spread is observed, with the highest mobility being $\mu = 2.7$ cm^2/V s. An optical micrograph (100× magnification) of isolated plate like crystallites formed within the confined space (b). At the edge of the film needle like crystals are formed within the reservoirs. The inset shows a crystallite at 500× magnification. The straight and regularly shaped edges are an indication for a single crystal nature, but this needs yet to be determined by crystallographic measurements.

2.3. C_{60}

C_{60} exhibited high field-effect mobilities in transistors when thermally evaporated as thin films or in single crystal devices grown from vapor phase [45–49]. However, thin films from solution are hard to prepare due the tendency for three-dimensional growth and clustering of C_{60} molecules while the solvents slowly evaporate after spin coating or drop casting. The limited space in the *z*-direction in the deposition technique presented here might limit the clustering of C_{60} and enhance in-plane order.

Spin coating of the C_{60} solution rendered discontinuous films and could therefore not be used as a reference. Due to a higher boiling point of both solvents (*m*-xylene and carbontetrachloride) used for fabrication of C_{60} thin films, a longer waiting time was required for the solvent to evaporate. Annealing is not possible during the deposition due to a small deformation of the stamp and the consequent wetting of the substrate at the channel region. Isolated crystals were formed and oriented towards the edge of the channel (Fig. 7b). Needle like crystallites at the edge of the film were often observed and originated in the reservoirs. Underneath the stamp in the confined space the crystallites were flat with a thickness of ~30–40 nm, which was determined by AFM (see Fig. S8, Supplementary information). Long straight steps observed on top of the crystal, with a height of 1–2 nm, suggest a step of a single C_{60} molecular layer, but a single crystal nature needs yet to be determined by crystallography. Cross polarized light microscopy is not possible due to the isotropic nature of C_{60}. The absence of a continuous film is due to the limited solubility of C_{60} and thus, the amount of material present in the confined space. Au electrodes were thermally evaporated on top of the isolated crystallites, which resulted in two or three transistors per sample. The *W*/*L* ratio was measured by optical microscopy, where the width *W* is determined by the sum of the crystallite widths of the crystallites bridging the gap between the source and drain electrode and *L* being the distance between the electrodes, see Supplementary information for more details. The saturated field-effect mobilities obtained for 15 devices are plotted in Fig. 7a. A large spread in mobilities of two orders of magnitude is observed, which is likely due to a combination of variation in crystallite thickness, shape, orientation and contact quality to the crystallites. The maximum mobility measured was $\mu = 2.7$ cm^2/V s for device 11 (see Fig. S1 and S9, Supplementary information). This is about twice the value of the highest mobility measured for n-type organic transistors from solution with $\mu = 1.4$ cm^2/V s [50]. The mobility is still lower compared to that by thermal evaporation [47,48,51]. This might be due to solvent inclusion in the crystallites [52], which can alter the packing structure. To identify the reason for a lower mobility, further characterization of the crystal structure is needed. It is also important to fabricate closed layers of C_{60} crystals, which might be achieved by multiple deposition steps, a better control of the spacing between stamp and substrate, or a change of solvent.

3. Conclusions

We demonstrated a solution deposition technique for the fabrication of single crystals and crystalline films. A limited adhesion between a fluorinated rigid stamp and substrate facilitates the formation of a confined space that enables crystallization of organic thin films. The versatility of the technique was demonstrated by using small molecules and a polymer. Advantages of this technique include the small amount of material required per sample and the possibility of using solvents with a low boiling point while achieving an ordered packing. The drawback of small material amounts is the high concentration required for the formation of a continuous film, which might therefore be limited by the solubility of the material.

P3HT formed an in-plane oriented crystalline thin film when processed by confined solution deposition. The

field-effect mobility measured, $\mu = (2.7 \pm 0.8) \times 10^{-2}$ cm^2/V s, was an order of magnitude higher than those obtained from spin coated films under similar conditions from chloroform, due to an improved in-plane packing of the molecules.

TIPS-pentacene formed large elongated crystals from a low boiling point solvent with a high field-effect mobility $\mu = 0.29 \pm 0.14$ cm^2/V s. Different types of crystals are formed on a single substrate, varying in thickness and size.

Isolated crystallites of C_{60} showed mobilities up to $\mu = 2.7$ cm^2/V s, twice as high as previously reported for n-type organic materials. The limited solubility of C_{60} prevents the formation of a continuous thin film and processing C_{60} by confined solution deposition will require further optimization.

We expect our technique to lead to further studies on crystalline films, exhibiting high field-effect mobilities, and possibly to the emergence of the ability to fabricate single crystal FETs on a large scale, for example by making large stamps on isolated small pillars while the majority of the stamp is suspended above the substrate. Many parameters, like channel geometry and solvent, can be optimized for each material under study in the near future to obtain large single crystals or large crystalline domains.

4. Methods

The molds for perfluoropolyether (PFPE) stamps were made by fabricating line features (height ~150 μm) of SU-8 photoresist onto a silicon wafer. The lines varied in width between 1 and 4 mm and have a length between 8 and 15 mm. The PFPE was mixed with 0.05% acetophenone photoinitiator for photocrosslinking. After casting the PFPE in an N_2-atmosphere, the films were photocrosslinked by UV irradiation (ELC-500, Lightning Enterprises) in a chamber using a total power of 36 W at a distance of approximately 10 cm. Each irradiation lasted 30 s with a 1 min cooling interval to ensure full crosslinking. This was repeated five or six times, depending on the amount of PFPE. To fabricate different channel geometries for patterned films, a protective adhesive sheet, normally used for wafer dicing, is placed on a wafer. From the dicing sheet the required stamp geometries are drawn and cut, and the redundant pieces are removed by hand. This results, albeit with low resolution due to manual cutting, in stamps where only the shape of the channel is modified, i.e., the region that is in close proximity with the substrate.

Highly doped Si wafers with a 300 nm thermally grown oxide were used as a substrate and functioned simultaneously in FETs as a common gate electrode, with the SiO_2 being the dielectric. The SiO_2 was treated with HMDS by spin coating at 3000 rpm and subsequent rinsing with 2-propanol. The absence of a surface treatment of the oxide, or when processed on rougher glass substrates, did not lead to a difference in film formation. When the contact angle of a surface treatment was too high, i.e., close to the contact angle of the PFPE stamp, films will delaminate upon removing the stamp. Samples were fabricated and measured in air for TIPS-pentacene (Sigma–Aldrich) and in N_2 atmosphere for C_{60} (Sigma–Aldrich) and P3HT, to prevent degradation.

Electronic grade regio-regular P3HT was purchased from Merck Chemicals (Lisicon SP001, Mw = 44 kDa). Reference films were fabricated with P3HT from chloroform (5 mg/ml) by spin coating at 2500 rpm to compare with those made by the confined solution deposition technique (also with 5 mg/ml in chloroform). TIPS-pentacene (Sigma–Aldrich) thin films were prepared from chloroform with a concentration of 20 mg/ml. For the solution of C_{60} (Sigma–Aldrich) we used a mixture of carbon tetrachloride and *m*-xylene (4:3) as a solvent with a concentration of 0.8 mg/ml. After sonication for 30 min and filtering with a 0.2 μm PTFE filter, the films were fabricated in a glovebox under nitrogen atmosphere.

After dissolving the semiconductor material, the solution (5–10 μl) was deposited at the edge of the confined space and is immediately dispensed underneath the stamp by capillary forces. Thermal evaporation (Angstrom Engineering) of the Au source and drain electrodes, with a thickness of 40 nm and *W*/*L* of 20 with $L = 50$ μm, was done through a shadow mask at a rate of 0.5–1.0 Å/s^{-1} at a pressure $P \leqslant 10^{-6}$ mbar. Electrical characterization of the electronic devices was done with a Keithley 4200 semiconductor analyzer. Morphology and crystallinity were studied by optical microscopy (Leica, DM4000M) and tapping mode AFM (Veeco, MultiMode Scanning Probe Microscope). GIXD measurements were performed at the Stanford Synchrotron Radiation Lightsource, using beamline 11-3 [53]. The scattering intensity was detected on a 2D image plate and the incident angle was set between 0.10° and 0.12° to optimize the signal-to-background ratio.

Acknowledgments

The authors acknowledge Guarav Giri (Gino) and Hanying Li for assistance and technical discussions. HBA acknowledges the Netherlands Organisation for Scientific Research (NWO) for support. CJB was funded by a Ruth L. Kirschstein NIH fellowship. Financial support by NSF DMR Solid State Chemistry Program (Grant number DMR-0705687-002). Portions of this research were carried out at the Stanford Synchrotron Radiation Lightsource, a Directorate of SLAC National Accelerator Laboratory and an Office of Science user Facility operated for the US Department of Energy Office of Science by Stanford University.

Appendix A. Supplementary data

Supplementary data associated with this article can be found, in the online version, at doi:10.1016/j.orgel.2011.11.005.

References

[1] T. Sekitani, H. Nakajima, H. Maeda, T. Fukushima, T. Aida, K. Hata, T. Someya, Nat. Mater. 8 (2009) 494–499.
[2] G.H. Gelinck, H.E.A. Huitema, E. van Veenendaal, E. Cantatore, L. Schrijnemakers, J.B.P.H. van der Putten, T.C.T. Geuns, M. Beenhakkers, J.B. Giesbers, B.-H. Huisman, E.J. Meijer, E.M. Benito, F.J. Touwslager, A.W. Marsman, B.J.E. van Rens, D.M. de Leeuw, Nat. Mater. 3 (2004) 106–110.
[3] E. Cantatore, T.C.T. Geuns, G.H. Gelinck, E. van Veenendaal, A.F.A. Gruijthuijsen, L. Schrijnemakers, S. Drews, D.M. de Leeuw, IEEE J. Solid-State Circuits 42 (2007) 84–92.

[4] T. Sekitani, T. Yokota, U. Zschieschang, H. Klauk, S. Bauer, K. Takeuchi, M. Takamiya, T. Sakurai, T. Someya, Science 326 (2009) 1516–1519.
[5] A.N. Sokolov, M.E. Roberts, O.B. Johnson, Y. Cao, Z. Bao, Adv. Mater. 22 (2010) 2349–2353.
[6] M.-J. Spijkman, J.J. Brondijk, T.C.T. Geuns, E.C.P. Smits, T. Cramer, F. Zerbetto, P. Stoliar, F. Biscarini, P.W.M. Blom, D.M. de Leeuw, Adv. Funct. Mater. 20 (2010) 898–905.
[7] V. Podzorov, E. Menard, A. Borissov, V. Kiryukhin, J.A. Rogers, M.E. Gershenson, Phys. Rev. Lett. 93 (2004).
[8] O.D. Jurchescu, J. Baas, T.T. Palstra, Appl. Phys. Lett. 84 (2004) 3061.
[9] T. Hasegawa, J. Takeya, Sci. Technol. Adv. Mater. 10 (2009) 024314.
[10] R. Pfattner, M. Mas-Torrent, I. Bilotti, A. Brillante, S. Milita, F. Liscio, F. Biscarini, T. Marszalek, J. Ulanski, A. Nosal, M. Gazicki-Lipman, M. Leufgen, G. Schmidt, L.W. Molenkamp, V. Laukhin, J. Veciana, C. Rovira, Adv. Mater. 22 (2010) 4198–4203.
[11] J. Takeya, M. Yamagishi, Y. Tominari, R. Hirahara, Y. Nakazawa, T. Nishikawa, T. Kawase, T. Shimoda, S. Ogawa, Appl. Phys. Lett. 90 (2007) 102120.
[12] A.L. Briseno, S.C.B. Mannsfeld, M.M. Ling, S. Liu, R.J. Tseng, C. Reese, M.E. Roberts, Y. Yang, F. Wudl, Z. Bao, Nature 444 (2006) 913–917.
[13] S.C.B. Mannsfeld, A.L. Briseno, S. Liu, C. Reese, M.E. Roberts, Z. Bao, Adv. Funct. Mater. 17 (2007) 3545–3553.
[14] Y. Li, C. Liu, A. Kumatani, P. Darmawan, T. Minari, K. Tsukagoshi, AIP Adv. 1 (2011) 022149.
[15] D.H. Kim, D.Y. Lee, H.S. Lee, W.H. Lee, Y.H. Kim, J.I. Han, K. Cho, Adv. Mater. 19 (2007) 678–682.
[16] J.-P. Hong, S. Lee, Angew. Chem. Int. Edit. 48 (2009) 3096–3098.
[17] R.Z. Rogowski, A. Dzwilewski, M. Kemerink, A.A. Darhuber, J. Phys. Chem. C 115 (2011) 11758–11762.
[18] K. Nakayama, Y. Hirose, J. Soeda, M. Yoshizumi, T. Uemura, M. Uno, W. Li, M.J. Kang, M. Yamagishi, Y. Okada, E. Miyazaki, Y. Nakazawa, A. Nakao, K. Takimiya, J. Takeya, Adv. Mater. 23 (2011) 1626–1629.
[19] H. Minemawari, T. Yamada, H. Matsui, J. Tsutsumi, S. Haas, R. Chiba, R. Kumai, T. Hasegawa, Nature 475 (2011) 364–367.
[20] S.C.B. Mannsfeld, A. Sharei, S. Liu, M.E. Roberts, I. McCulloch, M. Heeney, Z. Bao, Adv. Mater. 20 (2008) 4044–4048.
[21] H.A. Becerril, M.E. Roberts, Z. Liu, J. Locklin, Z. Bao, Adv. Mater. 20 (2008) 2588–2594.
[22] Z. Liu, Hé.A. Becerril, M.E. Roberts, Y. Nishi, Z. Bao, IEEE Trans. Electron Dev. 56 (2009) 176–185.
[23] M. Cavallini, F. Biscarini, Nano Lett. 3 (2003) 1269–1271.
[24] M. Cavallini, P. Stoliar, J.-F. Moulin, M. Surin, P. Leclère, R. Lazzaroni, D.W. Breiby, J.W. Andreasen, M.M. Nielsen, P. Sonar, A.C. Grimsdale, K. Müllen, F. Biscarini, Nano Lett. 5 (2005) 2422–2425.
[25] C.J. Bettinger, H.A. Becerril, D.H. Kim, B.-L. Lee, S. Lee, Z. Bao, Adv. Mater. 23 (2011) 1257–1261.
[26] J.P. Rolland, R.M. Van Dam, D.A. Schorzman, S.R. Quake, J.M. DeSimone, J. Am. Chem. Soc 126 (2004) 2322–2323.
[27] J.N. Lee, C. Park, G.M. Whitesides, Anal. Chem. 75 (2003) 6544–6554.
[28] R.J. Kline, M.D. McGehee, E.N. Kadnikova, J. Liu, J.M.J. Fréchet, M.F. Toney, Macromolecules 38 (2005) 3312–3319.
[29] D.M. DeLongchamp, B.M. Vogel, Y. Jung, M.C. Gurau, C.A. Richter, O.A. Kirillov, J. Obrzut, D.A. Fischer, S. Sambasivan, L.J. Richter, E.K. Lin, Chem. Mater. 17 (2005) 5610–5612.
[30] H. Yang, T. Joo Shin, Z. Bao, C.Y. Ryu, J. Polym. Sci. B Polym. Phys. 45 (2007) 1303–1312.
[31] S. Cho, K. Lee, J. Yuen, G. Wang, D. Moses, A.J. Heeger, M. Surin, R. Lazzaroni, J. Appl. Phys. 100 (2006) 114503.
[32] J. Liu, Y. Sun, X. Gao, R. Xing, L. Zheng, S. Wu, Y. Geng, Y. Han, Langmuir 27 (2011) 4212–4219.
[33] M. Aryal, K. Trivedi, W. (Walter) Hu, ACS Nano 3 (2009) 3085–3090.
[34] D.A. Lyashenko, A.A. Zakhidov, V.A. Pozdin, G.G. Malliaras, Org. Electron. 11 (2010) 1507–1510.
[35] K.-J. Baeg, D. Khim, D.-Y. Kim, J.B. Koo, I.-K. You, W.S. Choi, Y.-Y. Noh, Thin Solid Films 518 (2010) 4024–4029.
[36] J.-F. Chang, B. Sun, D.W. Breiby, M.M. Nielsen, T.I. Sölling, M. Giles, I. McCulloch, H. Sirringhaus, Chem. Mater. 16 (2004) 4772–4776.
[37] J. Huang, J. Sun, H.E. Katz, Adv. Mater. 20 (2008) 2567–2572.
[38] F. Dinelli, M. Murgia, P. Levy, M. Cavallini, F. Biscarini, D. de Leeuw, Phys. Rev. Lett. 92 (2004).
[39] J.E. Anthony, J.S. Brooks, D.L. Eaton, S.R. Parkin, J. Am. Chem. Soc. 123 (2001) 9482–9483.
[40] C.W. Sele, B.K.C. Kjellander, B. Niesen, M.J. Thornton, J.B.P.H. van der Putten, K. Myny, H.J. Wondergem, A. Moser, R. Resel, A.J.J.M. van Breemen, N. van Aerle, P. Heremans, J.E. Anthony, G.H. Gelinck, Adv. Mater. 21 (2009) 4926–4931.
[41] T. Sakanoue, H. Sirringhaus, Nat. Mater. 9 (2010) 736–740.
[42] S.K. Park, T.N. Jackson, J.E. Anthony, D.A. Mourey, Appl. Phys. Lett. 91 (2007) 063514.
[43] J. Kim, J. Jeong, H.D. Cho, C. Lee, S.O. Kim, S.-K. Kwon, Y. Hong, J. Phys. D Appl. Phys. 42 (2009) 115107.
[44] S.C.B. Mannsfeld, M.L. Tang, Z. Bao, Adv. Mater. 23 (2011) 127–131.
[45] R.C. Haddon, A.S. Perel, R.C. Morris, T.T.M. Palstra, A.F. Hebard, R.M. Fleming, Appl. Phys. Lett. 67 (1995) 121.
[46] A. Dodabalapur, H.E. Katz, L. Torsi, R.C. Haddon, Science 269 (1995) 1560–1562.
[47] T.D. Anthopoulos, B. Singh, N. Marjanovic, N.S. Sariciftci, A. Montaigne Ramil, H. Sitter, M. Colle, D.M. de Leeuw, Appl. Phys. Lett. 89 (2006) 213504.
[48] X.-H. Zhang, B. Domercq, B. Kippelen, Appl. Phys. Lett. 91 (2007) 092114.
[49] Y. Kubozono, S. Haas, W.L. Kalb, P. Joris, F. Meng, A. Fujiwara, B. Batlogg, Appl. Phys. Lett. 93 (2008) 033316.
[50] J.H. Oh, S.-L. Suraru, W.-Y. Lee, M. Könemann, H.W. Höffken, C. Röger, R. Schmidt, Y. Chung, W.-C. Chen, F. Würthner, Z. Bao, Adv. Funct. Mater. 20 (2010) 2148–2156.
[51] A. Virkar, S. Mannsfeld, J.H. Oh, M.F. Toney, Y.H. Tan, G.-Yu. Liu, J.C. Scott, R. Miller, Z. Bao, Adv. Funct. Mater. 19 (2009) 1962–1970.
[52] D. Schindler, M. Felsmann, E. Weber, Acta Crystallogr. C 66 (2010) o361–o363.
[53] S.C.B. Mannsfeld, A. Virkar, C. Reese, M.F. Toney, Z. Bao, Adv. Mater. 21 (2009) 2294–2298.